A Neural-Network-Based Fault Diagnosis Approach for Analog Circuits by Using Wavelet Transformation and Fractal Dimension as a Preprocessor

Wenji Zhu, Yigang He

Abstract—This paper presents a new method of analog fault diagnosis based on back-propagation neural networks (BPNNs) using wavelet decomposition and fractal dimension as preprocessors. The proposed method has the capability to detect and identify faulty components in an analog electronic circuit with tolerance by analyzing its impulse response. Using wavelet decomposition to preprocess the impulse response drastically de-noises the inputs to the neural network. The second preprocessing by fractal dimension can extract unique features, which are the fed to a neural network as inputs for further classification. A comparison of our work with [1] and [6], which also employs back-propagation (BP) neural networks, reveals that our system requires a much smaller network and performs significantly better in fault diagnosis of analog circuits due to our proposed preprocessing techniques.

Keywords—Analog circuits, fault diagnosis, tolerance, wavelet transform, fractal dimension, box dimension.

I. INTRODUCTION

ANALOG fault diagnosis has been an active area of research since the mid-1970s with significant work carried out at the system, board, and chip level [1-5]. The application of neural networks to this area is very appealing since no model or comprehensive examination of these effects is requred [6-12]. In this approach, the fault features extraction technique is one of the most important steps in the whole diagnosis process. Fractal theory has been widely used in the fault diagnosis of mechanical and electric power systems as a preprocessor and great performance have been achieved [6-11]. However, it is still rare that fractal theory was applied in analog fault diagnosis. Fractal theory is applied in fault feature extraction for analog circuits in [2], and good results has been achieved. However, the abscissa and the vertical coordinate of

the sampling data in plane are time or frequency, and voltage or the amplitute of transfer function, which are two different variables. Thus, directly using square grid to cover the sampling curves will sometimes reduce the fault diagnosis accuracies and even get wrong fault diagnosis results.In this work, normalization will be first used to the abscissa and the vertical coordinate. After then, the box dimension of the normalized data will be calculated.

Considering the effects of the noise and tolerance, if the box dimensions of sampled data are directly extracted from the impulse response of a circuit under test (CUT) as the fault features, it is difficult to meet the requirements in practice. [6] shows that wavelet transformation is a powerful tool in signal-denoising. And the relevant studies [7-9] also found that wavelet transfomation and fractal theory are both based on self-similarity and are the same in the object-recognized process, which is a process from coarse to fine. So, in this paper, t he circuit's impulse response will be first preprocessed by wavelet transformation. And then, use normalization and fractal theory to generate features for training the neural network. Comparison of our work with [6] in a later section clearly indicates the effectiveness of our proposed method and that our proposed method improves the accuracies of analog fault diagnosis..

The material in this paper is arranged in the following order. In Section II, we briefly discuss wavelet transformation used in this paper. The box dimension is discussed in Section III. In Section IV, our proposed preprocessing techniques for analog-circuit fault diagnosis are discussed. Section V covers the neural network architecture appropriate for our analog fault diagnosis method. Two illustrations to demonstrate the strength of our diagnosis technique are given in Section VI. The conclusions are presented in Section VII.

II. WAVELET TRANSFORM

Wavelet is a limited function in time and frequency domain. Using wavelet function to multiply the original signal is actually to add a window to it. The definition of wavelet transformation is the innner product of different sale a and shift τ of mother wavelet $\psi(t)$, and the signals $x(t)$ to be analyzed [5], that is

World Academy of Science, Engineering and Technology
International Journal of Electronics and Communication Engineering
Vol:4, No:8, 2010

$$WT_x(a,\tau) = \frac{1}{\sqrt{a}}\int_{-\infty}^{+\infty} x(t)\psi^*\left(\frac{t-\tau}{a}\right)dt, a>0 \qquad (1)$$

The equivalent representation of (1) in frequency domain is as follows.

$$WT_x(a,\tau) = \frac{\sqrt{a}}{2\pi}\int_{-\infty}^{+\infty} X(\omega)\psi^*(a\omega)e^{j\omega}d\omega \qquad (2)$$

Where $X(\omega)$ and $\psi(\omega)$ are the Fourier transformations of $x(t)$ and $\psi(t)$, respectively.

In applying wavelet analysis to sampled signals, one needs to perform the downsampling operation after each level of decomposition to preserve the number of data points in the orginal signal. This simply means to include every other data point in the signal components (approximation and detail). Consequently, the number of data points in the components at level j approximation or detail will be reduced by a factor of two compared to the corresponding number of data points at level $(j-1)$.

III. BOX DIMENSION

Assume that F is a non-empty and bounded set in $\mathbf{R}^n$ and $N_\delta(F)$ is the minimum number of boxes with maximum diameter δ, which can cover the set F, the lower and inferior limits of box dimension can be defined as

$$\underline{\dim}_B F = \varliminf_{\delta \to 0} \frac{\ln N_\delta(F)}{-\ln \delta} \qquad (3)$$

$$\overline{\dim}_B F = \varlimsup_{\delta \to 0} \frac{\ln N_\delta(F)}{-\ln \delta} \qquad (4)$$

If the lower and inferior limits of the box dimension are equal, the box dimension of F can be rewritten as

$$\dim_B F = \lim_{\delta \to 0} \frac{\ln N_\delta(F)}{-\ln \delta} \qquad (5)$$

In order to calculate the box dimension of set F in plane $\mathbf{R}^2$, draw the square grids with the length being δ in plane, first. Then, calculate the number of the square grids at the intersection of set F. Finally, mark the points constituted by different δ and its relevant $N_\delta(F)$ in double-logarithmic coordinate $\ln \delta^{-1} - \ln N_\delta(F)$, which is shown in Fig.1. The slope of the line in Fig.1 is the approximated value of box dimension of F.
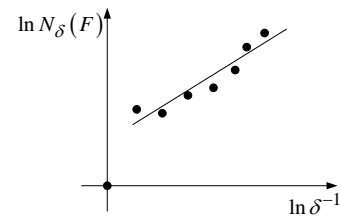

Fig.1. The estimation of the box dimension of F set

For the fault diagnosis of analog circuits, the abscissa and the vertical coordinate of the sampled data in plane are time or frequency, and voltage or the amplitute of transfer function, which are two different variables. Thus, using improved square-grid based method to cover the sampled curves includes the following four steps.

Step1. Normalize the abscissa and the vertical coordinate of the sampled curve and then embed the sampled curve into the unit squares.

Step2. Select a group of squares with the length being δ_m, where $m = 1, 2, \cdots, M$. The maximum and minimum of δ_m are 0.2 and 2/N, where N is the number of sampled points for each concerned curve.

Step 4. Use unit squares with length being δ_m to cover the curve and calculate the number of the square N_m at the intersection of the curve.

Step 5. Draw the curve of $\ln(N_m) - \ln(\delta_m)$, where $m = 1, 2, \cdots, M$. If the concerned curve is fractal, the curve constituted by the points of $(\ln(\delta_m), \ln(N_m))$ is a straight line with least-square method. The slope of straight line is the box dimension.

IV. PREPROCESSING TECHNIQUES

Since only the output terminal is accessible for most application in practice, so wavelet transformation and fractal dimension based fault feautre extraction method are obtained by the calculation of CUTs' outputs in this paper. First, de-noise and decompose the impulse responses of CUTs based on wavet decompostion. Then, calculate box dimension of the decomposed data according to Section III. The block diagram of the feature extraction process is listed in Fig.2.
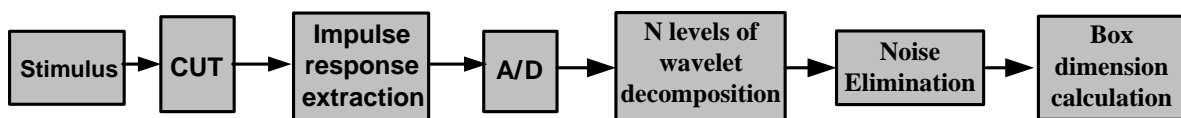

Fig.2. The block diagram of fault feature extraction process

It can be seen from Fig.2 that the fault feature extraction process includes the following steps:

1)Perform sensitivity analysis on CUTs to determine fault classes.

2)Denoise and decompose the impulse responses of the CUTs for each fault classes.

3) Calculate the box dimensions of decomposed signals.

The box dimension are then fed to a neural network as inputs for further classification.

V. NEURAL NETWORK CLASSIFIER DESIGN

The neural network selected in our work is multilayer back-propagation (BP) neural network, which is mainly used in

World Academy of Science, Engineering and Technology
International Journal of Electronics and Communication Engineering
Vol:4, No:8, 2010

pattern recognition, function approximation, classification, etc. The structure of BPNN is shown in Fig.3, where $X = [x_1, x_2, \cdots x_r, \cdots x_R]$, $r = 1, 2, \cdots, R$ is the input vector. R is the number of the input-layer neurons; $\omega 1_{ir}$ is the weight between i^{th} hidden-layer neuron and r^{th} input-layer neuron; $\omega 2_{ji}$ is the weight between j^{th} output-layer neuron and i th hidden-layer neuron.

$B1 = [b_1, b_2, \cdots, b_i, \cdots, b_{S1}]$, $i = 1, 2, \cdots, S1$ is the bias vector of hidden-layer neurons; $S1$ is the number of hidden-layer

neurons; $B2 = [b_1, b_2, \cdots, b_j, \cdots, b_{S2}]$, $j = 1, 2, \cdots, S2$ is the bias vector of output-layer neurons; $S2$ is the number of output-layer neurons; The activation functions of hidden- and output-layer neurons are $f1$ and $f2$, which are sigmoid and linear functions, respectively. $Y = (y_1, y_2, \cdots, y_{S2})$ and $T = (t_1, t_2, \cdots, t_{S2})$ are the actual and target output vectors of the network.
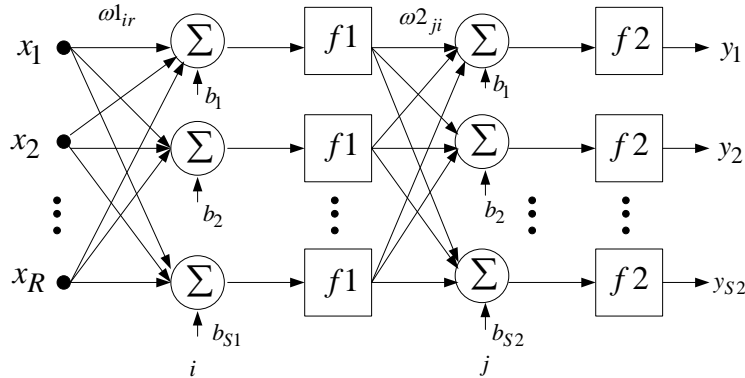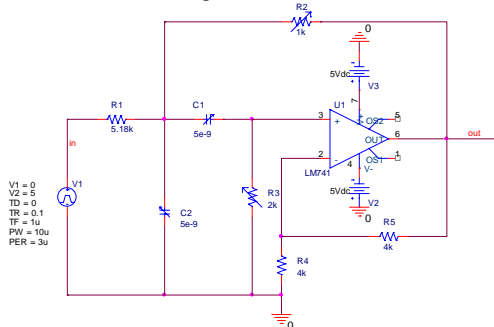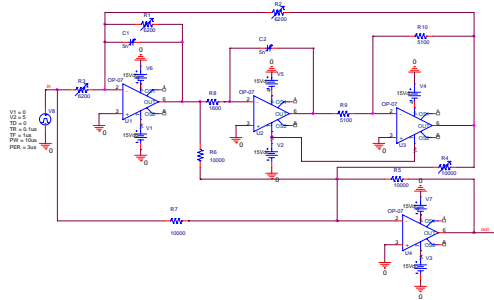

Fig.3. The structure of BP neural network

VI. EXAMPLE CIRCUITS AND METHOD APPLICATION

A. Sample Circuits and Faults

In order to verify the correctness of our proposed method, the softwares of Matlab 7.1 and OrCAD10.5 are adopted to simultate the circuits in Figs.4 (a) and (b).

(a) 25kHzSallen-Key bandpass filter

(b) Four op-amp biquad high-pass filter
Fig.4. The circuit under test

The nominal values for the components in Figs.4 (a) and (b) are shown in the Figures. A test signal is applied to the CUTs .

The frequency responses with the components set to their nominal vaules are shown in Figs.5 (a) and (b). The nomimal centre frequency and 3db cut-off frequecy of the two CUTs are 25kHz and17.60667kHz, which are obtained by performance index analysis. The impulse response of these circuits with resistors and capacitors allowed to vary within tolerances of 5% and 10% belongs to the no-fault (NF) class.
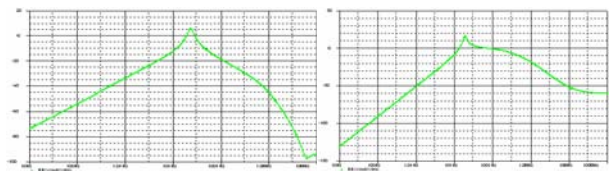
(a)The frequency response of Fig.4(a) (b) The frequency response of 4(b)
Fig.5. The amplitude-frequency distribution of the CUTs

A component sensitivity analysis is performed on the CUT in Fig. 4(a) to identify critical single faults. The sensitivity ranking of the discrete components to centre frequency is : R_3, C_2, R_2, and C_1. So, when R_3, C_2, R_2, and C_1 are 50% higher or lower than the nominal values shown in Fig4(a), we get the fault classes $R_3 \uparrow$, $R_3 \downarrow$, $C_2 \uparrow$, $C_2 \downarrow$, $R_2 \uparrow$, $R_2 \downarrow$, $C_1 \uparrow$, $C_1 \downarrow$, and NF. In this notation, $\uparrow$ and $\downarrow$ stand for high and low, respectively. An input pulse with $V1 = 0$, $V2 = 5V$, $TD = 0$, $TR = 0.1 \mu s$, $TF = 1 \mu s$, $PW = 10 \mu s$, and $PER = 3 \mu s$ to the filer input are applied. The output node (out) is utilized to obtain the circuit impulse response.

The second circuit studied in this paper is more complicated and is shown in Fig.4 (b). This is a four-operational-amplifier

World Academy of Science, Engineering and Technology
International Journal of Electronics and Communication Engineering
Vol:4, No:8, 2010

biquad high-pass filter. The fault classes include $C_1\uparrow$, $C_1\downarrow$, $C_2\uparrow$, $C_2\downarrow$, $R_1\uparrow$, $R_1\downarrow$, $R_2\uparrow$, $R_2\downarrow$, $R_3\uparrow$, $R_3\downarrow$, $R_4\uparrow$, $R_4\downarrow$, and NF., where $\uparrow$ and $\downarrow$ stand for higher and lower than nominal values by 50%,respectively.

B. Feature Extraction

When one component are 50% higher or lower than the nominal values shown in Figs.4(a) and (b) and the other elements of the CUTs fall into their tolerance ranges, the fault features can be extracted by the analysis of the impulse response of the CUTs, which constitutes the following.
1) For the nominal circuits, conduct transient analysis on the CUT under each fault classes to obtain the impulse response of the CUT. Denoise and decompose the impulse response by wavelet decomposition. Calculate the box dimensions of the decomposed signals using the software of Matlab7.1.
2) For the tolerance circuits, conduct Monte Carlo and transient analyses on the CUT to obtain the impulse response of the CUT. Denoise and decompose the impulse response by wavelet decomposition. Calculate the box dimensions of the decomposed signals using the software of Matlab7.1. The box dimensions obtained in (1) and (2) will be fed to the neural network as its inputs.

C. Neural Network Classifier

Based on the aforementioned analysis, the network architecture can be designed to have six inputs, nine outputs, and eighteen hidden neurons for the CUT in Fig.4(a); and six inputs, 13 outputs, and 26 hidden neurons for the CUT in

Fig.4(b). Assume that T={0,…,0,1,0,…,0}is the target ouput vector. When j^{th} fault class feature occurs, T_j is equal to 1, and the other outputs are equal to zero. The features, which are extracted by performing one time of transient analysis for the nominal circuit and 40 times of Monte Carlo and transient analyses on the tolerance circuits, are sent to the neural network in batch to adjust its weights and biases, that is, the diagnosis errors are calculated after all the features sent to the neural network. The weight adaptation equation is given by:

$$\Delta\mathbf{W}_p^{(r)} = \sum_{k=1}^{N}\Delta\mathbf{W}_{p,k}^{(r)} = \eta\sum_{k=1}^{N}e_{p,k}^{(r)}\hat{\mathbf{h}}_k^{(r-1)}\ \ (r=1,2,\cdots,R)\quad(6)$$
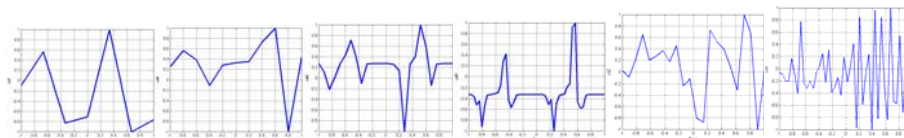
Where N is the number of features; $e_{p,k}^{(r)}$ is the difference of rth feature between j^{th} actual output $y_{p,k}^{(r)}$ and the target output $t_{p,k}^{(r)}$, that is, $e_{p,k}^{(r)}=t_{p,k}^{(r)}-y_{p,k}^{(r)}$; η is the learning rate and $0<\eta<1$; and $\hat{\mathbf{h}}_k^{(r-1)}$ is the output vector in $(r-1)^{th}$ hidden-layer.
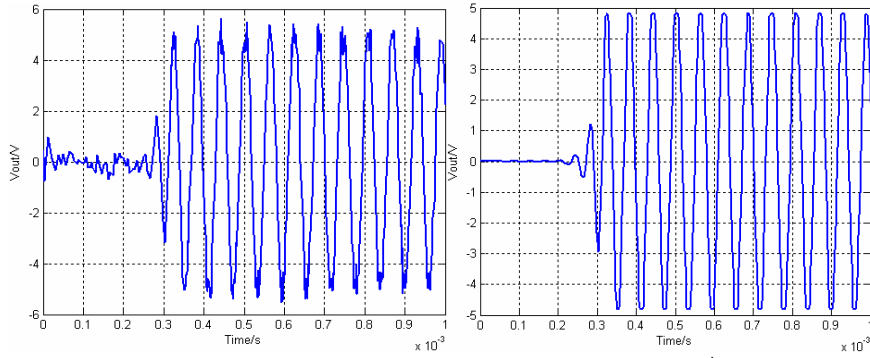
D. Results and Analysis

Using the proposed method, we have studied the fault diagnosis of analog circuits in Figs.4(a) and (b). Parts of the simulation data of the two circuits without tolerance are listed in Tables I (a) and (b) and Figs.6 and 7. These are acheived by using 5 levels of haar wavelet decomposition to denoise and decompose the circuits' outputs.
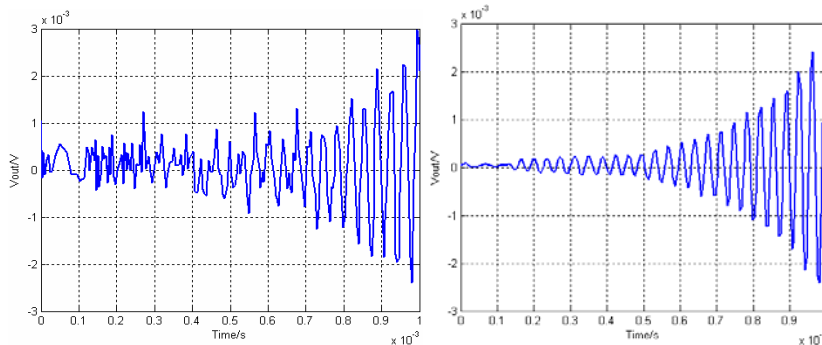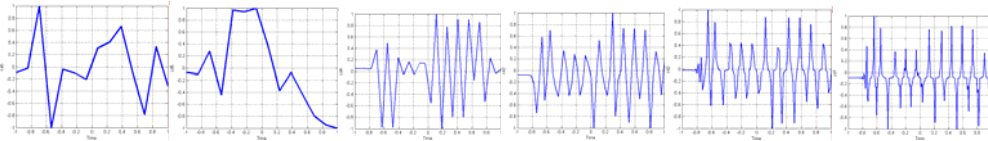

(a) The outputs and denoised outputs of Fig.4 (a) with NF

(b) The five levels of wavelet decomposed signals of Fig.4 (a)with NF

World Academy of Science, Engineering and Technology
International Journal of Electronics and Communication Engineering
Vol:4, No:8, 2010

(c) The outputs and denoised outputs of Fig.4 (a) with R_2 ↑

(d) The five levels of wavelet decomposed signals of Fig.4 (a) with R_2 ↑

Fig.6. The outputs, denoised outputs and their corresponding wavelet decomposed signals in Fig.4 (a) with parts of fault classes

(a) The outputs and denoised outputs ofFig.4 (b) R_1 ↑

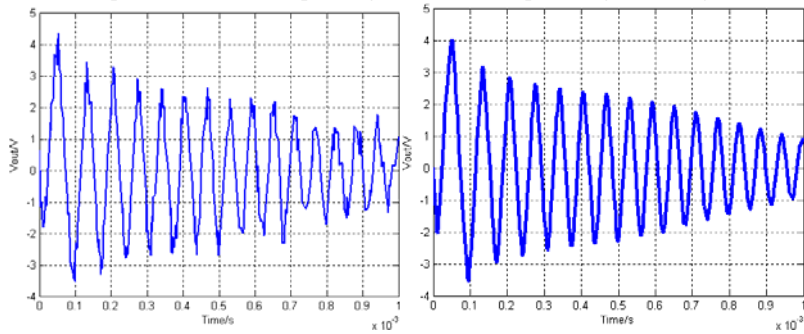(b) The five levels of wavelet decomposed signals of Fig.4 (b) R_1 ↑

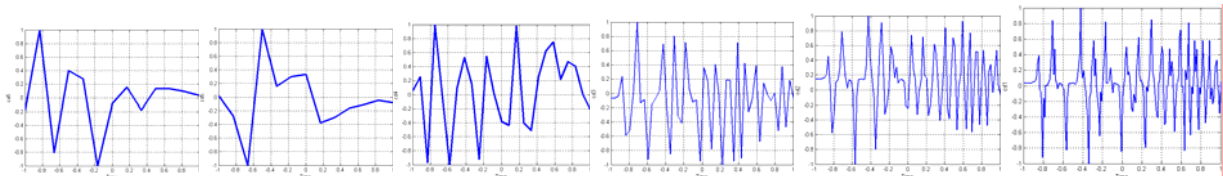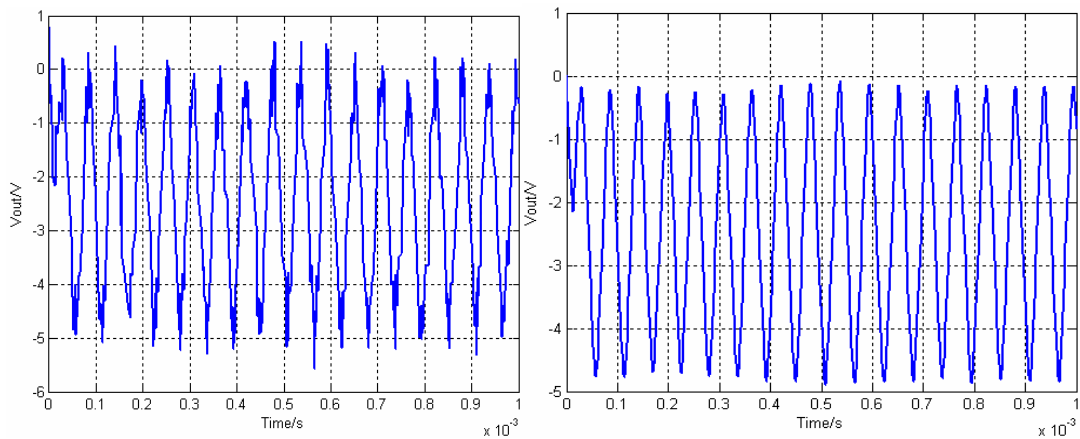(c) The outputs and denoised outputs ofFig.4 (b) with R_4 ↓

(d) The five levels of wavelet decomposed signals of Fig.4 (b)with $R_4 \downarrow$

Fig.7. The outputs, denoised outputs and their corresponding wavelet decomposed signals in Fig.4 (b) with parts of fault classes
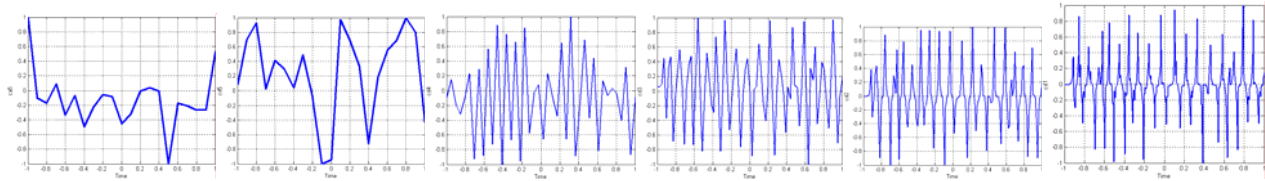
TABLEI. THEMAXIMUM COEFFICIENTS OF THE DECOMPOSED IMPULSE RESPONSE

(a) THE MAXIMUM COEFFIENTS OF THE DECOMPOSED IMPULSE RESPONSES FOR THE NOMINAL CIRCUIT OF FIG.4 (a)

Maximun Coeffients / Fault Classes	Max(ca5)	Max(cd5)	Max(cd4)	Max(cd3)	Max(cd2)	Max(cd1)
NF	0.0002	0	0	0	0	0
$R_3 \uparrow$	0.0989	0.0686	0.0706	0.1026	0.0197	0.0127
$R_3 \downarrow$	0.0011	0	0	0	0	0
$C_2 \uparrow$	0.0002	0	0	0	0.0001	0
$C_2 \downarrow$	0.0083	0.0035	0.0045	0.0049	0.0017	0.0008
$R_2 \uparrow$	0.0002	0	0	0	0	0
$R_2 \downarrow$	13.0055	26.2243	15.2669	5.8104	3.2883	1.5156
$C_1 \uparrow$	0.0002	0	0	0.0001	0.0002	0.0001
$C_1 \downarrow$	0.0002	0	0	0	0	0

(b) THE MAXIMUM COEFFIENTS OF THE DECOMPOSED IMPULSE RESPONSES FOR THE NOMINAL CIRCUIT OF FIG.4 (a)

Maximum Coefficients / Fault Classes	Max(ca5)	Max(cd5)	Max(cd4)	Max(cd3)	Max(cd2)	Max(cd1)
NF	2.8735	10.9022	6.5145	-2.7182	-1.2174	0.2782
$C_1 \uparrow$	2.8792	13.8682	7.4977	4.5818	-1.1745	0.6577
$C_1 \downarrow$	-2.3511	1.7973	-5.3919	1.9863	-0.8899	-0.2941
$C_2 \uparrow$	29.4238	5.1900	8.8482	-2.4474	1.6001	0.6525
$C_2 \downarrow$	2.8791	10.0066	8.0901	-3.2732	1.3476	-0.6622
$R_1 \uparrow$	29.4204	5.1904	8.8483	-2.4479	1.6001	0.6528
$R_1 \downarrow$	-2.8941	5.1696	-2.7607	-2.3636	-0.5615	0.4617
$R_2 \uparrow$	20.7859	-8.1281	-10.2783	-2.9137	-1.444	0.4612
$R_2 \downarrow$	-19.0801	-12.1212	7.8653	2.6182	-1.1621	-0.6695
$R_3 \uparrow$	-10.8898	-5.2036	7.4581	1.8889	0.9242	-0.3608
$R_3 \downarrow$	35.9117	-15.612	7.0667	-3.2697	1.2145	0.7852
$R_4 \uparrow$	-9.5158	8.2452	-3.9897	-1.5114	-0.8221	-0.3336
$R_4 \downarrow$	29.4238	5.1902	8.8482	-2.4484	1.6001	0.6526

In Figs.6 and 7, the data in horizontal and vertical axis are all normalized. As shown in Figs.6 and 7, it can be seen that using haar wavelet to denoise the impulse responses has achieved great performance. In addition, the decomposed signals have fractal characteristics, so that fractal theory can be applied on the issues. In Table I, Max (ca5), Max (cd5), Max (cd4), Max (cd3), Max (cd2) and Max (cd1) represent the maximum ones of the wavelet coefficients ca5, cd5, cd4, cd3, cd2 and cd1. The data in Tables I (a) and (b) show that the fault features of NF, $R_2 \uparrow$ and $C_1 \downarrow$ extracted by wavelet decomposition are all the same, which means that these faults cannot be uniquely identified. In addition, the features of $C_2 \uparrow$ and $C_1 \uparrow$ are very close to those mentioned above, which means the two fault classes cannot be identified, either.

The features for the nominal circuits of Figs. 4(a) and (b) extracted by wavelet decomposition and box dimension are listed in Tables II (a) and (b).

World Academy of Science, Engineering and Technology
International Journal of Electronics and Communication Engineering
Vol:4, No:8, 2010

TABLE II BOX DIMENSIONS FOR EACH LEVEL OF WAVELET DECOMPOSITION

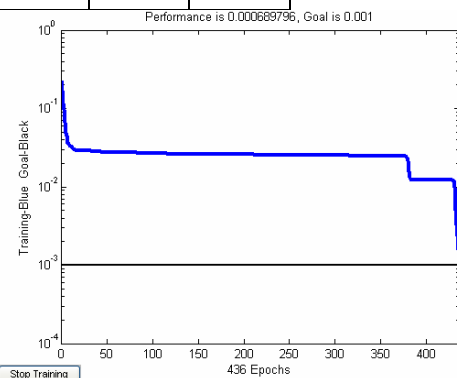(a) BOX DIMENSIONS FOR EACH LEVEL OF WAVELET DECOMPOSITION FOR THE CIRCUIT IN FIG.4(a)

Box Dimension / Fault Classes	BD(ca5)	BD(cd5)	BD(cd4)	BD(cd3)	BD(cd2)	BD(cd1)
NF	1.2729	1.4227	1.5337	1.6911	1.7270	1.9335
$R_3 \uparrow$	1.2295	1.3959	1.6959	1.5295	1.6244	1.8704
$R_3 \downarrow$	1.3307	1.3307	1.4206	1.4591	1.6550	1.8658
$C_2 \uparrow$	1.2604	1.2604	1.4783	1.7041	1.7523	1.8743
$C_2 \downarrow$	1.0206	1.2266	1.7446	1.8614	1.8766	1.8902
$R_2 \uparrow$	1.6826	1.8295	1.8296	1.9024	1.9307	1.9535
$R_2 \downarrow$	1.1911	1.2244	1.5229	1.5937	1.6125	1.6572
$C_1 \uparrow$	1.1911	1.4478	1.5922	1.5923	1.7250	1.8922
$C_1 \downarrow$	1.0704	1.1534	1.2763	1.3512	1.3652	1.6602

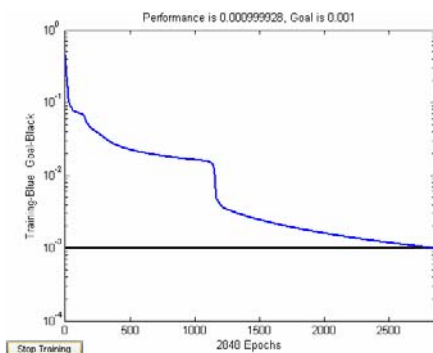(b) BOX DIMENSIONS FOR EACH LEVEL OF WAVELET DECOMPOSITION FOR THE CIRCUIT IN FIG.4 (b)

Box Dimension / Fault Classes	BD(ca5)	BD(cd5)	BD(cd4)	BD(cd3)	BD(cd2)	BD(cd1)
NF	1.1534	1.2922	1.2922	1.2963	1.5091	1.7074
$C_1 \uparrow$	1.0244	1.0244	1.1911	1.3512	1.3512	1.3922
$C_1 \downarrow$	1.1920	1.4829	1.7426	1.7425	1.8534	1.8534
$C_2 \uparrow$	1.2244	1.2704	1.3704	1.5436	1.7534	1.9091
$C_2 \downarrow$	1.1911	1.2337	1.3370	1.4669	1.5643	1.6335
$R_1 \uparrow$	1.2602	1.2922	1.5841	1.6743	1.7630	1.7756
$R_1 \downarrow$	1.1746	1.3133	1.3704	1.3837	1.6922	1.8478
$R_2 \uparrow$	1.1614	1.3478	1.4244	1.4333	1.6922	1.9911
$R_2 \downarrow$	1.1911	1.5121	1.6743	1.7604	1.7959	1.8819
$R_3 \uparrow$	1.1917	1.2244	1.2911	1.2436	1.2763	1.3223
$R_3 \downarrow$	1.1614	1.2434	1.2917	1.3074	1.4550	1.7074
$R_4 \uparrow$	1.2206	1.3244	1.3922	1.4370	1.5920	1.6922
$R_4 \downarrow$	1.2917	1.2922	1.5304	1.5418	1.6922	1.8307

In Table II, BD(ca5), BD(cd5), BD (cd4), BD (cd3), BD (cd2) and BD (cd1) represent the box dimensions of the wavelet coefficients ca5, cd5, cd4, cd3, cd2 and cd1. The data in TablesII(a) and (b) show that the fault features of different fault classes are different, which means that these faults can be uniquely identified.

For circuits with tolerance, ambiguity may occur. For the circuits in Figs.4(a) and (b), resistors and capacitors are assumed to have tolerance values of 5% and 10%, respectively. The ambiguity groups for different fault classes of the circuits in Figs.4(a) and (b) can be obtained by 40 times of Monte Carlo analysis, respectively. Our simulation results show that all the nine (including normal) fault classes in the circuit of Fig.4(a) and all the thirteen fault classes in the circuit of Fig.4 (b) are falling into different ambiguity groups, and thus, the fault identifiability of the circuit are both 100%. The method in [7] cannot distinguish between NF and for the circuit in Fig.4(a). Obviously, the method proposed in this paper has a higher correct fault recognition rate.


(a) The training curves of the neural networks for the circuit in Fig.4 (a)

World Academy of Science, Engineering and Technology
International Journal of Electronics and Communication Engineering
Vol:4, No:8, 2010

(b) The training curves of the neural networks for the circuit in Fig.4 (b)

Fig.8. The training curves

The performance analysis of the neural network classifier of the circuits in Figs.4(a) and (b) are shown in Figs.8(a) and (b). Figs.8 (a) and (b) show that the training goals are obtained through 436 and 2848 epochs. Figs.9 (a) and (b) illustrate that the percentages for wrong diagnosis are less than 1% and 1.5% for the circuits in Figs.4 (a) and (b) when the noise is lower than 0.3. From the Figs.9 (a) and (b), we can see that the networks can reach at least 99% and 98.5% of accurate diagnoses for the circuits in Figs.4 (a) and (b).
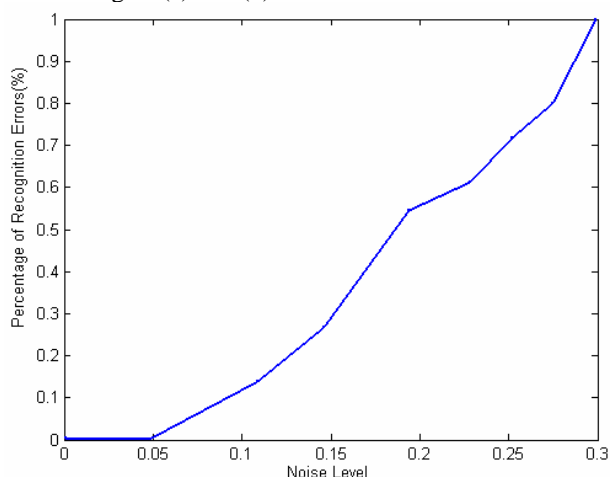
(a) The relationship of diagnosis error for inputs with noise for the circuit in Fig.4(a)
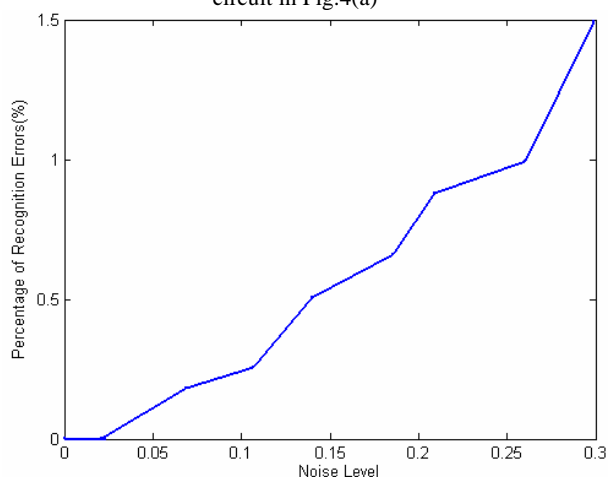
(b) The relationship of diagnosis error for inputs with noise for the circuit in Fig.4(b)

Fig.9. The relationship of diagnosis error for inputs with noise

In [1], a three-layer BP neural network without any preprocessors was used to perform diagnosis on the CUT in Fig.4 (a). The network has 49 inputs, ten first-layer neurons, and ten second-layer neurons, resulting in a total adjustable parameter of about $659(49X10+10X10+49+10+10)$. The training of the network will consume a lot of computing time. Using wavelet decomposition and box dimension as preprocessors for the inputs of the neural network, we need only six inputs, eighteen first-layer neurons, and nine outputs for the circuit in Fig.4(a), and there are only about 303 $(6X18+18X9+6+18+9=303)$ parameters to be adjustable. Thus, the number of weights and biases of the network in this paper is reduced, which directly leads to shorter training time.

The method in [6] cannot distinguish between $R_1 \uparrow$ and NF, $C_2 \downarrow$ and $R_4 \uparrow$ for the circuit in Fig.4(a), and has 97% correct classification for the circuit in Fig.4(b). However, our trained neural networks has 99% correct classification for the test data extracted from the circuit of Fig.4 (a) and only misclassified three test data out of the 40 test data for $C_2 \uparrow$ in the circuit of Fig.4 (b). Also, our proposed method achieves 98.5% accuracy in classifying fault components for the circuit in Fig.4(b). Obviously, compared with [6], the proposed method in this paper has a higher correct fault recognition rate.

VII. CONCLUSION

The back-propagation neural networks with wavelet transformation and fractal dimension as preprocessors to fault diagnosis of analog circuits have been applied in this paper. Our study indicates that the proposed preprocessing techniques have a significant impact on analog fault diagnosis due to the selection of an optimal number of relevant features. This leads to neural network architectures with minimal size that can be trained efficiently and carry out fault diagnosis with a higher degree of accuracy.

REFERENCES

[1] Robert Spina, Shambhu Upadhyaya, "Linear circuit fault diagnosis using neuromorphic anlayzers", IEEE transactions on circuits and systems-II: analog and digital signal processing, Vol.44, No.3, March 1997,pp188-196.
[2] Xiaobai Mao, Liheng Wang, Changxi Li, "SVM classifier for analog fault diagnosis using fractal features", Second international symposium on intelligent information technology application, pp553-557, 2008.
[3] Zhu wenji, He Yigang. A GA-BPNNs based approach for fault diagnosis of analog circuits and its application [J]. Journal of computer-aided design & computer graphics, Vol. 21, No. 9, pp1283- 1289, 2009.9.
[4] Zhu wenji, He Yigang.Neural network based soft fault diagnosis of analog circuits with tolerances [J]. Transactions of China Electrotechnical Society, Vol. 24, No. 11, pp184-191, 2009.11.
[5] Yanghong Tan, Yigang He, Chun Cui, and GuanyuanQiu, "A novel method for analog fault diagnosis based on neural networks and genetic algorithms", IEEE Transactions on Instrumentation and Measurement, Vol.57, No.11, pp2631-2639, November 2008.
[6] F. Aminian, M. Aminian, and H.W.Collins, "Analog fault diagnosis of actual circuits using neural networks", IEEE Trans. Instrum. Meas., Vol.51, No.3, pp.544-550, Jun. 2002.
[7] Liu Zhansheng, Liu Chengmin, Liu Shuchun, Fan Xianfeng, Tang Bingzhao, "Wavelet analysis and fractal geometry application to fault diagnosis of rotor friction between dynamic and static parts", Journal of Harbin Institute of Technology, Vol.31, No.1, pp55-56, 92, Feb.1999.

[8] Feisi r &d technology centre. Wavelet analysis and application with Matlab6.5. Beijing, China: Publishing House of Electronics Industry, 2003.1.
[9] Sha Zheng, Yuan Huojun. Fractal and Fitting Theories. ZheJiang University Press, 2005.3.
[10] Kenneth Falconer,Fractal Geometry: Mathematical Foundations and Applications, Published by Willey Publishing, Inc.,2003.
[11] Li Bicheng, Shao Meizhen, and Huang Jie, Pattern recognition theories and applications. Xian, China: University of Xian electronic science and technology, Press, 2008.